

Synthesis, physicochemical characterization, DFT calculation and biological activities of Fe(III) and Co(II)–omeprazole complexes. Potential application in the *Helicobacter pylori* eradication



Marcos G. Russo^a, Esteban G. Vega Hissi^b, Alberto C. Rizzi^c, Carlos D. Brondino^c, Ángel G. Salinas Ibañez^d, Alba E. Vega^d, Humberto J. Silva^d, Roberto Mercader^e, Griselda E. Narda^{a,*}

^a Química Inorgánica-INTEQUI, Facultad de Química, Bioquímica y Farmacia, Universidad Nacional de San Luis, Chacabuco y Pedernera-5700, San Luis, Argentina

^b Química Física-IMIBIO, Facultad de Química, Bioquímica y Farmacia, Universidad Nacional de San Luis, Chacabuco y Pedernera-5700, San Luis, Argentina

^c Departamento de Física, Facultad de Bioquímica y Ciencias Biológicas, Universidad Nacional del Litoral, Ciudad Universitaria, Paraje El Pozo, S3000ZAA Santa Fe, Argentina

^d Área de Microbiología, Facultad de Química, Bioquímica y Farmacia, Universidad Nacional de San Luis, Chacabuco y Pedernera-5700, San Luis, Argentina

^e Departamento de Física, Facultad de Ciencias Exactas, Universidad Nacional de la Plata-C.C. 67, 1900 La Plata, Argentina

HIGHLIGHTS

- The interaction between omeprazole (OMZ) and Fe(III) and Co(II) was studied.
- Fe(III)–OMZ and Co(II)–OMZ complexes were characterized by solid state techniques.
- The most favorable conformation for the complexes was obtained by DFT calculations.
- The compounds show antibacterial activities against *Helicobacter pylori*.
- Co(II)–OMZ shows a promising potential use for the treatment of gastric pathologies.

ARTICLE INFO

Article history:

Received 6 September 2013

Received in revised form 27 December 2013

Accepted 28 December 2013

Available online 8 January 2014

Keywords:

Metal–drug complexes

Omeprazole

Iron(III)

Cobalt(II)

DFT calculation

Antibacterial activity

ABSTRACT

The reaction between the antiulcer agent omeprazole (OMZ) with Fe(III) and Co(II) ions was studied, observing a high ability to form metal complexes. The isolated microcrystalline solid complexes were characterized by elemental analysis, X-ray powder diffraction (XRPD), Scanning Electron Microscopy (SEM), magnetic measurements, thermal study, FTIR, UV–Visible, Mössbauer, electronic paramagnetic resonance (EPR), and DFT calculations. The metal–ligand ratio for both complexes was 1:2 determined by elemental and thermal analysis. FTIR spectroscopy showed that OMZ acts as a neutral bidentate ligand through the pyridinic nitrogen of the benzimidazole ring and the oxygen atom of the sulfoxide group, forming a five-membered ring chelate. Electronic, Mössbauer, and EPR spectra together with magnetic measurements indicate a distorted octahedral geometry around the metal ions, where the coordination sphere is completed by two water molecules. SEM and XRPD were used to characterize the morphology and the crystal nature of the complexes. The most favorable conformation for the Fe(III)–OMZ and Co(II)–OMZ complexes was obtained by DFT calculations by using B3LYP/6-31G(d)&LanL2DZ//B3LYP/3-21G(d)&LanL2DZ basis set. Studies of solubility along with the antibacterial activity against *Helicobacter pylori* for OMZ and its Co(II) and Fe(III) complexes are also reported. Free OMZ and both metal complexes showed antibacterial activity against *H. pylori*. Co(II)–OMZ presented a minimal inhibitory concentration ~32 times lower than that of OMZ and ~65 lower than Fe(III)–OMZ, revealing its promising potential use for the treatment of gastric pathologies associated with the Gram negative bacteria. The morphological changes observed in the cell membrane of the bacteria after the incubation with the metal-complexes were also analyzed by SEM microscopy. The antimicrobial activity of the complexes was proved by the viability test.

© 2014 Elsevier B.V. All rights reserved.

* Corresponding author. Tel.: +54 266 4424689x6117.

E-mail address: gnarda@unsl.edu.ar (G.E. Narda).

1. Introduction

In the last decades coordination chemistry has been enriched due to the synthesis and characterization of a large number of transition metal complexes in which the metal is coordinated by functional groups present in most drugs [1–7]. There is an increasing knowledge that metal coordination modifies both drug adsorption and desorption [8,9] and biouptake [10], suggesting that the complex differs in its physicochemical properties from the ligand itself. Representative examples of this different behavior are the quinolone antibiotics, which show significant changes in activity upon metal coordination [11,12], the Co(II)–famotidine complex, which shows higher growth inhibitory activity against bacteria and fungi in comparison with the drug alone [7], and transition metal–omeprazole complexes, which, despite their biological activity against bacteria showed the same action as the pure drug, show better antifungal activity [13].

Advances in biocoordination chemistry are crucial to improve the design of drugs and to reduce the undesirable side effects, frequently associated with the presence of the metal. Transition metal complexes containing N-donor ligands (benzimidazole derivatives) have received a considerable attention in the last years as they constitute metal-based drugs exhibiting a high biological activity with reduced toxicity [14]. One of the most attractive features of these ligands is their structural similarity with pyrimidine and purine type nucleobases.

Omeprazole (Fig. 1), IUPAC name 5-methoxy-2-[[[4-methoxy-3,5-dimethyl-2-pyridinyl)methyl]sulphinil]1H-benzimidazole (OMZ), a substituted benzimidazole compound and prototype anti-secretory agent, is one of the employed proton pump inhibitors in the prophylaxis and treatment of gastroesophageal reflux disease, Zollinger–Ellison syndrome, gastric and duodenum ulceration, gastritis [15] and eradication of *Helicobacter pylori* (*H. pylori*). This bacterium is classified as group I carcinogen by the World Health Organization [16] and is recognized as a major etiological factor in the pathogenesis of gastritis peptic ulcer disease. The current most widely prescribed first-line regimen for *H. pylori* infection consists of two antibiotics and a proton pump inhibitor [17,18]. As this therapy is often accompanied by side effects along with the appearance of antibiotic resistance, the synthesis of new drugs for the treatment of these gastric diseases has growing interest.

Regarding the lack of accurate information about the nature of this kind of complexes [13], and the enormous scientific effort in the development of new antiulcerant compounds, we report the synthesis and characterization of two metal complexes of omeprazole with Fe(III) and Co(II) ions in order to determine the structure, physicochemical and antimicrobial properties. A more reliable structural description is provided by using a set of analytical and spectroscopic techniques. The crystalline nature of both complexes was determined by X-ray powder diffraction (XRPD) and Scanning Electron Microscopy (SEM). UV–Visible, Mössbauer, FTIR, and EPR

spectroscopies together with magnetic measurements were used to propose the coordination environment of the metal ions. Theoretical calculations using density functional theory (DFT) were performed to determine the lowest energy conformation of both complexes. Studies of solubility along with the antibacterial activity against *H. pylori* for Co(II) and Fe(III) complexes in comparison with pure OMZ are also discussed. SEM analysis of *H. pylori* with and without complexes, was performed to see the morphology changes on the cell membrane and the SEM images were consistent with MIC values. The antimicrobial nature was substantiated by the viability test.

2. Experimental

2.1. Materials

Omeprazole and metronidazole (MTZ) were purchased from Sigma–Aldrich® and Sigma Chemical, respectively, and used without any further purification. Clarithromycin (CLA) was provided by Laboratories ABBOT (Argentina). FeCl₃·6H₂O, CoCl₂·6H₂O and solvents were purchased from Merck. All chemicals and solvents were reagent grade and used as received.

2.2. Synthesis of the metal complexes

2.2.1. [Fe(OMZ)₂(H₂O)₂]Cl₃·2H₂O

A methanolic solution (70 mL) of OMZ (0.02 mmol, 69.08 mg) was added to a methanolic solution (20 mL) of FeCl₃·6H₂O (0.01 mmol, 27.03 mg) and the reaction mixture was stirred for 3 h at room temperature. The solution was filtered and left for slow evaporation. After a few days a red microcrystalline product was collected and washed with a water–methanol solution (1:1). Yield: 65% (67 mg). Anal. Found: C, 43.88; H, 4.02; N, 9.17; S, 6.78%. Calc. for C₃₄H₄₆N₆O₁₀S₂Cl₃Fe (MW: 925.22 g/mol): C, 44.09; H, 4.97; N, 9.07; S, 6.91%. (KBr, ν, cm⁻¹): ν(C–N)_{BZ}: 1637–1569, ν(C–N)_{PYR}: 1569, ν(S=O): 1065, ν(O–M): 557, ν(O–N): 464.

2.2.2. [Co(H₂O)₂(OMZ)₂]Cl₂·H₂O

An acetone solution (70 mL) of OMZ (0.02 mmol, 69.08 mg) was added to a N,N-dimethylformamide (N,N-DMF) solution (5 mL) of CoCl₂·6H₂O (0.01 mmol, 23.79 mg) and the reaction mixture was stirred for 3 h at room temperature. The solution was filtered and left for slow evaporation. After a few days a blue microcrystalline product was collected and washed with a water–acetone solution (1:1). Yield: 60% (55 mg). Anal. Found: C, 45.35; H, 4.88; N, 9.61; S, 7.13%. Calc. for C₃₄H₄₆N₆O₁₀S₂Cl₂Co (MW: 892.71 g/mol): C, 45.74; H, 5.19; N, 9.41; S, 7.18%. IR (KBr, ν, cm⁻¹): ν(C–N)_{BZ}: 1636–1573, ν(C–N)_{PYR}: 1572, ν(S=O): 1066, ν(O–M): 558, ν(O–M): 440.

2.3. Physicochemical measurements

Elemental analysis: C, H, N and S were estimated micro-analytically using a PERKIN ELMER 2400 elemental analyzer. The concentration of the metallic content in the complexes (dissolved in 1 N HCl) was assessed using an inductively coupled plasma optical emission spectrometer (ICP OES) model ICP-2070 from Baird, equipped with a 1-m Czerny–Turner monochromator and an ultrasonic nebulizer (USN) model U-5000 AT, with an on-line desolvation system. The ICP OES conditions were RF generator plasma power 1.0 kW; RF generator frequency, 40.68 MHz; gas flow rate, 8.5 L min⁻¹; auxiliary gas flow rate, 1 L min⁻¹; observation height-above load coil, 15 mm; wavelength (nm), Fe: II, 238.2, Co: II, 228.6. The USN experimental conditions were heater temperature, 140 °C; condenser temperature, 4 °C; and carrier gas

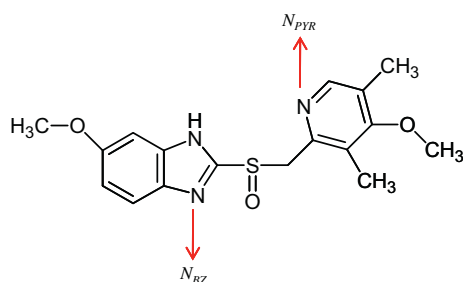


Fig. 1. Chemical structure of OMZ. N_{BZ} and N_{PYR} corresponding to pyridine nitrogen of benzimidazole ring and nitrogen of pyridine ring, respectively.

flow, 1 L min⁻¹. C₃₄H₄₆N₆O₁₀S₂Cl₃Fe: Anal. Found: 11.48%, calc.: 11.87%. C₃₄H₄₆N₆O₁₀S₂Cl₃Co: Anal. Found: 7.89%, calc.: 8.23%.

Magnetic susceptibilities of the complexes were measured by the Gouy method at room temperature using a Johnson Matthey, Alfa Products magnetic susceptibility balance. The effective magnetic moments were calculated from the expression $\mu_{\text{eff.}} = 2.828 (\chi_{\text{M}} T)^{1/2}$ B.M., where χ_{M} is the molar susceptibility corrected using Pascal's constants for the diamagnetism of all atoms in the compounds.

Thermogravimetric (TGA) and differential thermal analysis (DTA) curves were obtained with a Shimadzu TGA-51 Thermal Analyzer and DTA-50 Thermal Analyzer, using platinum pans, flowing air at 50 mL min⁻¹ and a heating rate of 10 °C min⁻¹ from room temperature to 1000 °C.

X-ray powder diffraction (XRPD) in a range of $2\theta = 3\text{--}50^\circ$ were obtained in reflection mode with a Rigaku D-MAX IIIIC diffractometer using Cu K α radiation (Ni-filter) and NaCl and quartz as external calibration standards.

Scanning Electron Microscopy (SEM) was used to observe and to analyze the morphology of the crystals, which were mounted on a double-sided carbon adhesive tape on gold-coated aluminum stubs (30 nm thickness) and processed in a standard sputter prior to observation in a LEO1450VP. In addition, the SEM morphological analysis of *H. pylori* was carried out from a HP270 inoculum prepared from 48 h culture and the suspension was adjusted to the tube 0.5 and 100 μL in 5 mL Mueller–Hinton broth. The cultures were incubated with OMZ, Fe(III)–OMZ and Co(II)–OMZ complexes (1 mg mL⁻¹ each) at 37 °C in microaerophilic atmosphere. After 26 h of incubation the samples were mounted on aluminum stubs and coated with a gold layer, processed in a standard sputter and then analyzed.

2.4. Spectroscopic methods

Fourier transformed infrared spectra (FTIR) were recorded on a Nicolet PROTÉGE 460 spectrometer provided with a CsI beamsplitter in the 4000–400 cm⁻¹ range with 64 scans and spectral resolution of 4 cm⁻¹, using the KBr pellet technique.

UV–Visible absorption spectra of OMZ and its metallic complexes dissolved in DMSO were measured with a Shimadzu UV-160 A recording spectrophotometer with a CPS-240A cell positioned using quartz cells (light-path = 10 mm); the temperature was maintained at 25.0 \pm 0.1 °C during the measurement.

Mössbauer spectroscopy was performed on a conventional constant acceleration spectrometer of 512 channels with a 50 mCi nominal activity ⁵⁷CoRh source in transmission geometry. The absorbers were powder samples of about 58 mg cm⁻² of the Fe(III) complex, calculated after the method described by Rancourt et al. [19] that yields the optimum absorber thickness. Isomer shifts were calibrated against an α -Fe foil at room temperature. Mössbauer spectra were analyzed with the Recoil program (version 1.05) [20].

X-band electronic paramagnetic resonance (EPR) spectra were obtained with a Bruker EMX plus spectrometer equipped with an Oxford Instruments helium-continuous flow cryostat, with 100 kHz field modulation and a modulation amplitude of 4.0 Gauss at 4.00 K for both complexes. The EPR parameters were obtained from spectral simulations of a powder sample using the program SimFonia (v. 1.25, Bruker Instruments Inc.).

2.5. Computational methods

Gaussian 03 [21] software package was employed to carry out all the quantum chemical calculations. DFT calculations were performed using the three-parameter exchange functional of Becke [22], in conjunction with the gradient corrected correlation

functional of Lee et al. [23]. The starting geometry of OMZ was obtained from crystallographic data available at CCDC [24]. Two OMZ conformers were built taking into account the accessibility of nitrogen atoms, N-pyridinic (N_{PYR}) and N-benzimidazolic (N_{BZ}) for a complexation reaction. Conformers geometries were optimized with the 6-31+G(d) and 6-31++G(d,p) basis sets [25] and natural charges were computed at the same level of theory within full Natural Bond Orbital (NBO) analysis, using NBO 3.1 [26] program implemented in Gaussian 03 [21]. Solvent effect was evaluated through geometry optimizations using the integral equation formalism polarizable continuum model (IEF-PCM) at B3LYP/6-31++G(d,p) level of theory.

The geometries of the different Fe(III)–OMZ and Co(II)–OMZ complexes were optimized using the standard 3-21G(d) basis set for hydrogen, carbon, oxygen, nitrogen and sulfur atoms and the Hay–Wadt small-core effective core potential (ECP) including a double- ζ valence basis set for iron, followed by single-point energy refinement with the 6-31G(d) basis set. This protocol has been employed previously for the calculations of other metal-complexes giving good results [27] and is designated as B3LYP/6-31G(d)&LanL2DZ//B3LYP/3-21G(d)&LanL2DZ.

In order to obtain a better agreement with the experimental data, the most stable Fe(III)–OMZ isomer was optimized further at B3LYP/6-31+G(d)&LanL2DZ level of theory. All stationary points were characterized by frequency calculations. To investigate the solvent effect of water on the metal complexes stability, single point calculations were performed using the IEFPCM model. Although continuum solvation models represent an approach resulting efficient and robust to be applied to the same systems studied in gas-phase [28,29].

2.6. Solubility assays

The quantitative solubility was spectrophotometrically determined in 0.1 N HCl pH 1 by the equilibrium solubility method. Saturated solutions of OMZ and its complexes were prepared by adding an excess of mass to a constant volume (5 mL) of medium. The saturated solutions were kept on a magnetic stirrer (100 rpm) in closed glass tubes for 12 h at 25 °C. Before the analysis, all samples were filtered through 0.45-mm Millipore PTFE filters. The calibration curve for OMZ obtained at 290 nm was used to calculate the concentration of the free drug. The Fe(III)–OMZ and Co(II)–OMZ complexes show absorption maxima at 288 and 289 nm, respectively, so the calibration curve used in OMZ was also used for the metal complexes. This UV–Visible method used to quantify the samples was linear in the 0.003–0.025 mg mL⁻¹ range, $R^2 = 0.999$. Statistical analysis was performed using one-way ANOVA followed by the Tukey post test. All results are expressed as the mean \pm S.E.M. of three measurements. Differences between means were considered significant at the $P < 0.05$ level.

2.7. Antibacterial activity

The antibacterial activity of OMZ and its metal complexes were studied against *H. pylori* NCTC 11638 reference strain obtained from the Microbiology Service of the Hospital Universitario de la Princesa, Madrid, Spain and clinical isolated strains HP796, HP270, HP271, HP277, HP294, HP295, HP299 obtained from gastric antral biopsy specimens.

The minimal inhibitory concentration (MIC) considered as the lowest concentration of the drug that inhibited the growth of *H. pylori* was determined by the conventional agar dilution method [30]. The tested compounds were dissolved in dimethylsulfoxide which has no inhibition activity. Twofold serial dilutions of the different compounds (10–0.016 mg mL⁻¹) were performed with 0.9% saline solution. The different *H. pylori* strain inoculums were prepared

from 48 h culture and the suspension was adjusted to the tube 0.5 of Mc Farland scale. Each bacterial suspension was spot inoculated (1.5 μL) onto petri dish of Mueller–Hinton agar supplemented with horse blood (MHA–HB) containing each compound assayed, and the MIC was determined following incubation at 37 $^{\circ}\text{C}$ for 3 days under microaerophilic conditions. DMSO was used as a control under the same condition for each organism.

MICs of CLA and MTZ were also determined using serial dilutions ranging from 128 to 0.008 $\mu\text{g mL}^{-1}$ [30]. Resistance was defined as the CLA MIC being 1 $\mu\text{g mL}^{-1}$ and MTZ MIC being 8 $\mu\text{g mL}^{-1}$. All samples were assayed by duplicate.

3. Results and discussion

3.1. FTIR analysis

The chemical formula of OMZ is shown in Fig. 1 [31]. Fig. S1, in Supplementary information, shows the FTIR spectra of OMZ, Fe(III)–OMZ and Co(II)–OMZ complexes while the proposed assignment of the vibrational modes are listed in Table 1. OMZ presents the $\nu(\text{N–H})$ located at 3426 cm^{-1} while the $\delta(\text{N–H})$ is centered at 1408 cm^{-1} , both in good agreement with the frequency values reported in the literature [32,33]. The $\nu(\text{N–H})$ is not observed in the complexes due to its overlap with a strong band assigned to the $\nu(\text{O–H})$ of coordinated and non-coordinated water molecules. However, the $\delta(\text{N–H})$ has shifted to lower frequency values in both complexes indicating the presence of imino hydrogen in the chelate compounds. The $\nu(\text{C=N})$ modes corresponding to the benzimidazole and pyridine rings are assigned at the 1650 and 1550 cm^{-1} region. The bands corresponding to the $\nu(\text{C=N})$ of the benzimidazole ring are located at 1627 and 1587 cm^{-1} for the free ligand [34], at 1637 and 1569 cm^{-1} for Fe(III)–OMZ and at 1636 and 1572 cm^{-1} for the complex Co(II)–OMZ. These shifts suggest the coordination of the metallic ion through the pyridinic nitrogen of the benzimidazole ring (N_{BZ}) [32]. No changes are observed in the $\nu(\text{C–N})$ of the OMZ pyridine ring in the spectra of the complexes, indicating that the pyridinic nitrogen (N_{PYR}) does not participate in the coordination to the metallic ion, as previously reported by Mohamed et al. [13]. A shift to lower frequencies is observed in $\nu(\text{S=O})$, from 1079 cm^{-1} for the free ligand to 1065 cm^{-1} and 1066 cm^{-1} for Fe(III)–OMZ and Co(II)–OMZ, respectively, which would indicate that the oxygen atom of the sulfoxide group is involved in the coordination. The infrared spectra of the complexes show new bands at 660–550 cm^{-1} and 470–400 cm^{-1} corresponding to $\nu(\text{O–M})$ and $\nu(\text{N–M})$, respectively [35,36] (Table 1). The analysis performed above suggests that OMZ acts as neutral bidentate ligand coordinating the metallic ion through N_{BZ} and the oxygen atom of the sulfoxide group.

Table 1
Selected vibrational modes of the FTIR spectra of OMZ, Fe(III)–OMZ and Co(II)–OMZ complexes.

| | OMZ (cm^{-1}) | Fe(III)–OMZ (cm^{-1}) | Co(II)–OMZ (cm^{-1}) |
|-----------------------------------|--|--|--|
| $\nu(\text{N–H})_{\text{bdz}}$ | (3426) _m | – | – |
| $\delta(\text{N–H})_{\text{bdz}}$ | (1408) _s | (1399) _w | (1397) _w |
| $\nu(\text{C=N})_{\text{bdz}}$ | (1627) _s (1587) _m | (1637) _s (1569) _s | (1636) _s (1572) _s |
| $\nu(\text{C=N})_{\text{pyr}}$ | (1568) _m | (1569) _s | (1572) _m |
| $\nu(\text{S=O})$ | (1079) _s | (1065) _m | (1066) _m |
| $\nu(\text{O–M})$ | – | (557) _{vw} | (558) _{vw} |
| $\nu(\text{N–M})$ | – | (464) _{vw} | (440) _{vw} |

s: Strong; m: medium; w: weak; vw: very weak; δ : deformation; ν : stretching.

3.2. Electronic and magnetic studies

The UV–Visible spectra of OMZ, Fe(III)–OMZ and Co(II)–OMZ are shown in Fig. S2. The electronic spectrum of the free ligand performed in DMSO shows two bands at 270 and 300 nm associated with $\pi\text{--}\pi^*$ transitions of the aromatic rings of OMZ. For both complexes, a slight shift of these bands to lower wavelengths evidences the coordination process. In addition, Fe(III)–OMZ exhibits two bands at 508 and 420 nm. The first one is in line with an octahedral geometry around the metal ion [37,38], while the

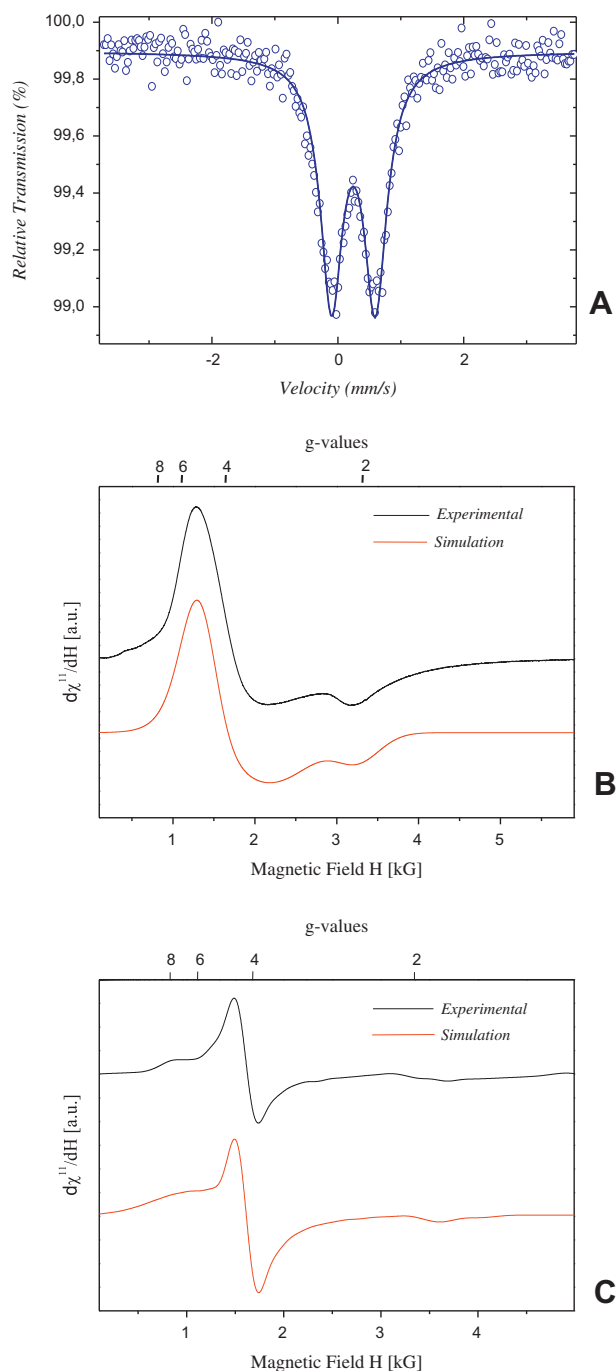


Fig. 2. Room temperature ^{57}Fe Mössbauer spectrum of $[\text{Fe}(\text{OMZ})_2(\text{H}_2\text{O})_2]\text{Cl}_3 \cdot \text{H}_2\text{O}$ (A); experimental and simulated EPR spectra of $[\text{Fe}(\text{OMZ})_2(\text{H}_2\text{O})_2]\text{Cl}_3 \cdot \text{H}_2\text{O}$ (B) and $[\text{Co}(\text{OMZ})_2(\text{H}_2\text{O})_2]\text{Cl}_2 \cdot \text{H}_2\text{O}$ (C) obtained at 9.475 GHz and 4 K. The linewidths for simulations were $\Delta B_x = 745$ G, $\Delta B_y = 150$ G and $\Delta B_z = 290$ G for Fe(III)–OMZ and $\Delta B_x = 370$ G, $\Delta B_y = 950$ G and $\Delta B_z = 550$ G for Co(II)–OMZ.

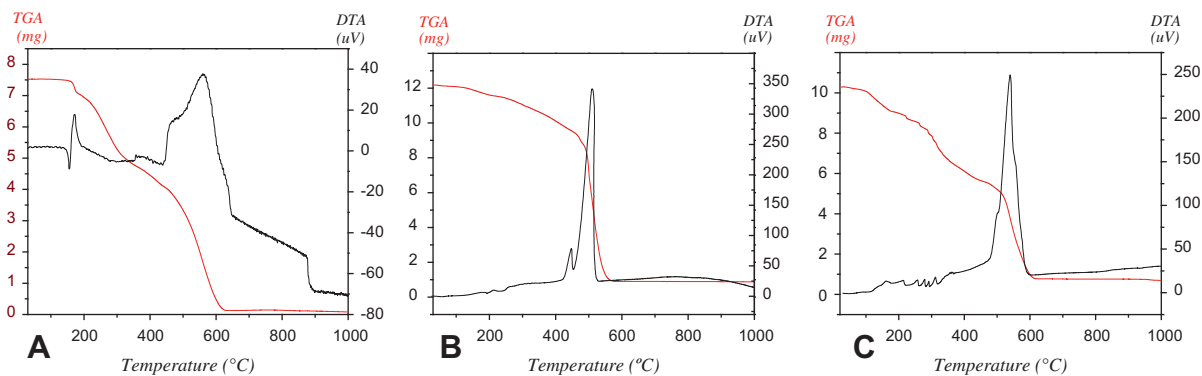


Fig. 3. TGA and DTA analysis of OMZ (A); Fe(III)-OMZ (B) and Co(II)-OMZ (C).

second one can be associated with a ligand-metal charge transfer (LMCT) band [39]. The value of the effective magnetic moment of 5.44 BM confirms the presence of high spin Fe(III) in octahedral environment.

The UV-Visible spectrum of Co(II)-OMZ shows, in addition to the bands from the ligand, three bands at 520, 425 and 395 nm. The two first absorptions are assigned to d-d transitions, compatible with an octahedral geometry around the metal ion [40], while the band located at 395 nm can be attributed to LMCT. The effective magnetic moment of 5.24 BM indicates the presence of high spin Co(II) in an octahedral environment [40].

3.3. Mössbauer and electron paramagnetic resonance spectroscopies

The Mössbauer spectrum of ^{57}Fe obtained for Fe(III)-OMZ at room temperature shows only a central well-defined doublet, indicating the presence of a single phase of Fe(III) (Fig. 2A). The isomer shift ($\delta = 0.35 \text{ mm s}^{-1}$), and the quadrupole splitting ($\Delta = 0.70 \text{ mm s}^{-1}$) are characteristic of high spin Fe(III) in a distorted octahedral geometry [41].

The EPR spectra of Co(II)-OMZ and Fe(III)-OMZ were collected at liquid helium temperatures, as indicated in the experimental section. Intense and well-defined signals were obtained at $T \sim 4 \text{ K}$ for both compounds. The EPR spectrum of Co(II)-OMZ is shown in Fig. 2B together with simulation. The g -values obtained by spectral simulation ($g_x = 4.89$, $g_y = 3.74$ y $g_z = 2.06$) are characteristic of high spin Co(II) ($S = 3/2$) with distorted octahedral coordination [42,43], where the highly anisotropic g -values are attributed to both spin-orbital interactions and to the effects of

the crystal field. No hyperfine structure, expected from 100% abundant ^{59}Co isotope ($^{59}I = 7/2$), is observed in the Co(II)-OMZ spectrum, suggesting the presence of exchange interactions between Co(II) ions mediated by the chemical path connecting the complex molecules. Fig. 2C shows the EPR spectrum of Fe(III)-OMZ complex together with simulation. The EPR parameters $g_x = 7.01$, $g_y = 4.27$ y $g_z = 1.68$; $D = 0.43 \text{ cm}^{-1}$, $E/D = 0.344$, where D and E are the axial and rhombic zero-field splitting parameters, respectively, were obtained by spectral simulation using a spin Hamiltonian with $S = 5/2$ and are characteristic of high spin Fe(III) ($S = 5/2$) with $E/D \approx 1/3$ in distorted octahedral coordination [44].

3.4. Thermal analysis

The thermal behavior of the metal complexes is clearly different from that of the pure ligand (Fig. 3). OMZ shows a first endothermic peak (158.77 °C) corresponding to the melting process, followed by an exothermic process (170.21 °C) attributed to the first event of thermal decomposition of the drug (Fig. 3A).

The thermal analysis of Fe(III)-OMZ shows a higher thermal stability relative to OMZ, which remains stable up to temperatures higher than 180 °C, and displays neither phase transition nor fusion (Fig. 3B). The DTA curve shows two successive endothermic peaks at 192.91 °C (27.71 J g^{-1}) and 231.22 °C (67.74 J g^{-1}), both processes associated with mass loss of 5.41% (calc 5.83%) in the TGA curve. These values are in agreement with the removal of one crystallization water molecule and of two coordination water molecules. Then, a continuous mass decay corresponding to

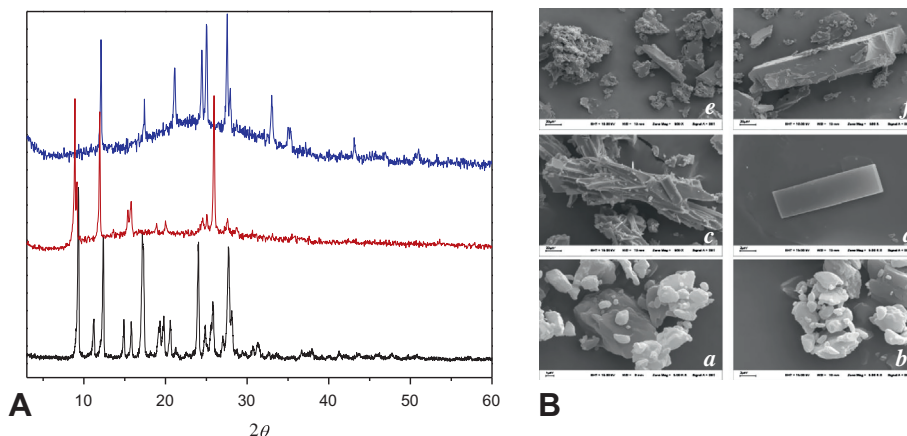


Fig. 4. A: X-ray powder diffractograms of OMZ (black), Fe(III)-OMZ (brown) and Co(II)-OMZ (blue). B: SEM microphotographs of OMZ (a and b: 5 kx), Fe(III)-OMZ (c: 500 x and d: 5 kx) and Co(II)-OMZ (e and f 500 x). (For interpretation of the references to colour in this figure legend, the reader is referred to the web version of this article.)

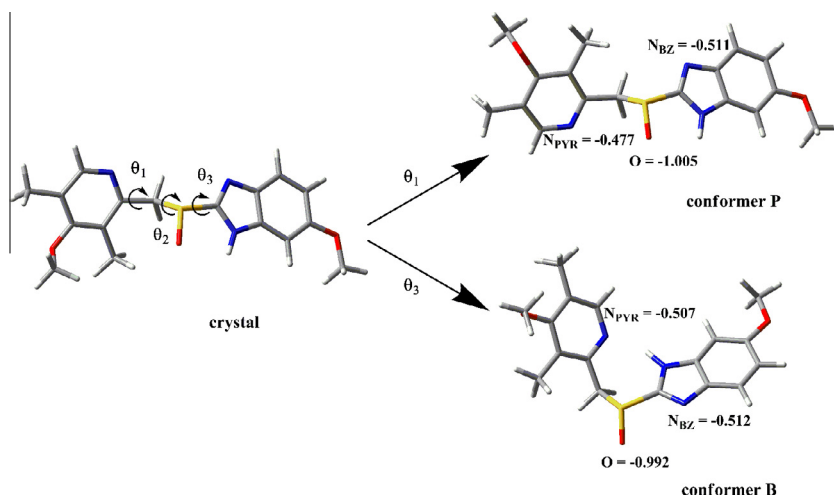


Fig. 5. Conformers P and B obtained by rotation in θ_1 or θ_3 angles respectively. The computed natural charges in both conformers at 6-31+G(d) and 6-31++g(3df,2p) level of theory are shown. The crystal structure was obtained from Ref. [24].

87.45% (calc 86.50%), consistent with the loss of three molecules of $\text{HCl}_{(g)}$ and two molecules of OMZ is observed. This mass loss is associated with two exothermal signals at 447.88 °C (266.34 J g^{-1}) and 510.34 °C (5.60 kJ g^{-1}) in the DTA curve. The final product of the oxidation process was Fe_2O_3 characterized by XRPD (PDF card: 898104 [45]). This analysis confirms that the stoichiometry of the Fe(III)–OMZ complex is $[\text{Fe}(\text{OMZ})_2(\text{H}_2\text{O})_2]\text{Cl}_3 \cdot \text{H}_2\text{O}$.

The thermal analysis of the Co(II)–OMZ (Fig. 3C) indicates a lower thermal stability of the complex relative to OMZ, which remains stable up to 112 °C. An endothermal signal is observed at 118.65 °C (298.08 J g^{-1}), which is related to a mass loss in the TGA curve of 13.55% (calc: 14.22%). This is in agreement with the loss of three water molecules (one of crystallization and two of coordination) together with the removal of two molecules of $\text{HCl}_{(g)}$. Then, a continuous mass loss of 79.013% (calc: 78.973%) is observed in the TGA curve associated with a strong DTA exothermal signal at 539 °C (7.30 kJ g^{-1}) corresponding to the loss of two molecules of the ligand, obtaining CoO as final product (PDF card:

750419 [45]). This analysis confirms that the stoichiometry of the Co(II)–OMZ complex is $[\text{Co}(\text{OMZ})_2(\text{H}_2\text{O})_2]\text{Cl}_2 \cdot \text{H}_2\text{O}$.

3.5. X-ray powder diffraction and SEM microscopy

X-ray powder diffraction patterns of OMZ, Fe(III)–OMZ and Co(II)–OMZ are shown in Fig. 4A. The diffraction peaks of OMZ are not observed in the diffractograms of the complexes indicating the formation of new crystalline phases. The SEM micro-photographies of OMZ and its metal complexes are shown in Fig. 4B. OMZ displays quasi-rectangular crystals, while Co(II)–OMZ and Fe(III)–OMZ exhibit a characteristic block shape.

3.6. DFT calculations

DFT calculations were performed for Fe(III)–OMZ and Co(II)–OMZ using cationic moiety of the complexes $[\text{M}(\text{OMZ})_2(\text{H}_2\text{O})_2]^{n+}$ (M: Fe(III), Co(II)). The Fe(III)–OMZ data is discussed here as a model.

3.6.1. Geometry of the ligand

Mohamed et al. [13] reported that the chelation process of OMZ to the metal ion could be achieved through N_{PYR} and O atoms of the sulfoxide group. However, according to our FTIR analysis (see Section 3.1 FTIR analysis), coordination occurs through N_{BZ} and O atom of the sulfoxide group. In order to re-evaluate the coordination sites, two possible conformers of the OMZ were proposed setting either θ_1 or θ_3 dihedral angles (Fig. 5) from the crystalline

Table 2

Dihedral angle values, electronic energy (E , hartree) and relative stability (ΔE , kcal mol^{-1}) of the crystal, conformer P and conformer B structures of OMZ computed at IEFPCM/B3LYP/6-31++G(d,p) level of theory.

| | θ_1 | θ_2 | θ_3 | E | ΔE |
|-------------|------------|------------|------------|--------------|------------|
| Crystal | 77.86 | −178.20 | 73.29 | −1447.397606 | 0.48 |
| Conformer P | −95.60 | −177.56 | 70.06 | −1447.397527 | 0.53 |
| Conformer B | 83.41 | −88.96 | −149.98 | −1447.398373 | 0.00 |

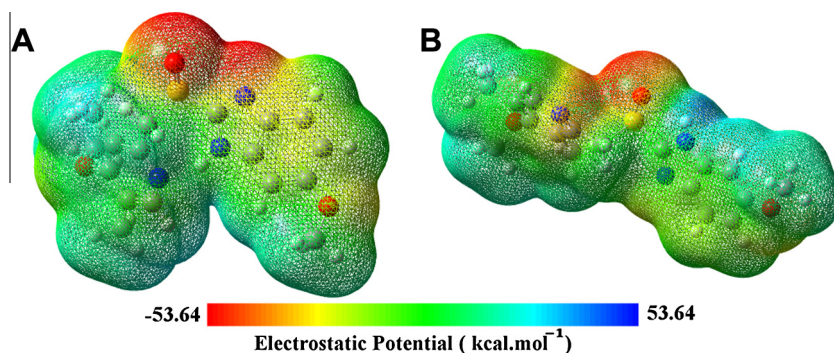


Fig. 6. Electrostatic potential map of conformers P and B.

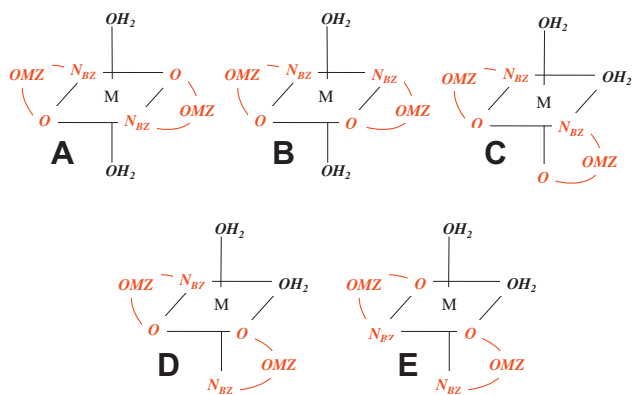


Fig. 7. M–OMZ (M: Fe(III) or Co(II)) isomers formulated for DFT calculations: (A) 2L, (B) 3L, (C) 2M, (D) 3M, and (E) 4M.

structure [24]. Conformer P was generated by setting coplanar the N_{PYR} and the O atom of the sulfoxide group (modifying θ_1 dihedral angle), and conformer B by setting coplanar the N_{BZ} and the O atom of the sulfoxide group (modifying θ_3 dihedral angle). Dihedral angles in addition to electronic energy values of the P and B conformers are listed in Table 2. Conformer B presents an intramolecular hydrogen bond between NH of the benzimidazole ring and N_{PYR} ; although this conformation is destabilized by torsional strain, it is the most stable one.

The N_{BZ} , N_{PYR} and the O atoms of the sulfoxide group were found to be the most negative centers and consequently, the best able to coordinate to the metal ion [46]. Natural charges of these atoms are presented in Fig. 5. N_{BZ} is more negative and therefore more basic than N_{PYR} when they are in the same plane as the O atom of the sulfoxide group. Moreover, as can be seen in the electrostatic potential (MEP) maps (Fig. 6), the negative surface over the O atom of the sulfoxide group and N_{BZ} (Conformer B, Fig. 6A) is larger than the negative surface over the O atom of the sulfoxide group and N_{PYR} (Conformer P, Fig. 6B).

Therefore, conformer B was selected to design the different complexes structures based on the following evidences: (a) the stability of a chelate is related to the number of atoms in the chelate ring, with the five-membered ring chelate being one of the most stable ones, as previously reported [47,48] (note that conformer B would lead to the formation of a five-membered ring chelate while the conformer P would form a six-membered ring chelate); (b) FTIR evidences described above (see Section 3.1 FTIR analysis); and (c) stability, natural charges and MEP calculations show that the conformer B is more appropriate for metal coordination.

3.6.2. Optimization of $[Fe(OMZ)_2(H_2O)_2]^{3+}$ and $[Co(OMZ)_2(H_2O)_2]^{2+}$ ions

In order to present a model for both complexes, five isomers were formulated and named as 2L, 3L, 2M, 3M and 4M (Fig. 7).

Table 3

Electronic energy values (E , hartree) and relative stability (ΔE , kcal mol⁻¹) of the five isomers proposed calculated at IEFPCM/B3LYP/6-31G(d)&LanL2DZ//B3LYP/3-21G(d)&LanL2DZ level theory.

| | 2L | 3L | 2M | 3M | 4M |
|--------------------|--------------|--------------|--------------|--------------|--------------|
| <i>Fe(III)–OMZ</i> | | | | | |
| E | –3170.492780 | –3170.478422 | –3170.486543 | –3170.487511 | –3170.486213 |
| ΔE | 0.00 | 9.01 | 3.91 | 3.31 | 4.12 |
| <i>Co(II)–OMZ</i> | | | | | |
| E | –3192.337786 | –3192.326726 | –3192.335481 | –3192.333917 | –3192.332971 |
| ΔE | 0.00 | 6.94 | 1.45 | 2.43 | 3.02 |

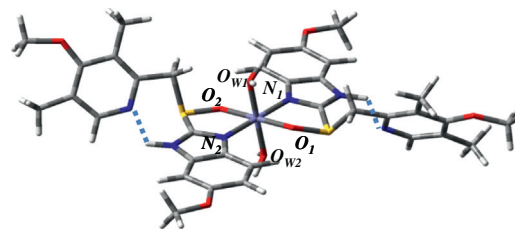


Fig. 8. Lowest energy model structure of 2L isomer. (O_{w1} and O_{w2} : oxygen atom of water molecules; O_1 and O_2 : oxygen atom of sulfoxide group of the ligand; N_1 and N_2 : N_{BZ} of the ligand).

Table 4

Selected bond lengths (Å) of the 2L isomer coordination polyhedron.

| 2L isomer | | OW1 | OW2 | O1 | O2 | N1 | N2 |
|---|---------|-------|-------|-------|-------|-------|----|
| <i>B3LYP/3-21G(d)&LanL2DZ level theory</i> | | | | | | | |
| Fe(III) | 1.95613 | 1.963 | 1.868 | 1.869 | 1.967 | 1.963 | |
| <i>B3LYP/6-31+G(d)&LanL2DZ level theory</i> | | | | | | | |
| Fe(III) | 2.124 | 2.123 | 2.061 | 2.035 | 2.023 | 2.015 | |

Electronic energy values and relative stabilities of the five isomers proposed for Fe(III) and Co(II)–OMZ complexes, are shown in Table 3, from which it can be derived that the stability of the complexes decreased in the next order: 2L, 3M, 2M, 4M and 3L for Fe(III)–OMZ while 2L, 2M, 3M, 4M and 3L for Co(II)–OMZ. As the 2L conformer is the most stable isomer for both complexes, only the corresponding to Fe(III)–OMZ is fully discussed here. Fig. S3 shows the optimized structures of 4M, 3M, 2M and 3L isomers for Fe(III)–OMZ and 2L, 3L, 2M, 3M and 4M for Co(II)–OMZ.

The intramolecular H-bond present in conformer B (see Section 3.6.1 *Geometry of the ligand*) remains in all the proposed isomers, what suggests that the repulsion effect between the OMZ ligands is the main contribution to the energy differences observed in the five isomers. The higher stability of 2L isomer is supported by the fact that the arrangement of the ligands minimizes the repulsion effects between them, as the aromatic rings are in *trans*-conformation. The most favorable conformation of the Fe(III)–OMZ is shown in Fig. 8. Although 4M, 3M, 2M and 3L isomers present repulsion effects between both ligands, and consequently a low stability, none of them can be excluded. The bond lengths of the coordination polyhedron in the 2L isomer are listed in Table 4. Since these lengths are not consistent with those reported for metal complexes of the d-block [49], the most stable 2L isomer was optimized at B3LYP/6-31+G(d)&LanL2DZ level of theory in order to obtain a better optimization. The new distances obtained are tabulated in Table 4, which shows that the distances between Fe(III) and the coordination sites obtained in this new optimization agree with those reported in literature [49]. They are indicative of a distorted octahedral geometry, as previously indicated by Mössbauer and EPR spectroscopies (see Section 3.3).

Table 5
MICs of OMZ and its metal complexes on *H. pylori* growth by agar dilution assay (mg mL⁻¹).

| Compounds | NCTC 11638 | HP796 | HP270 | HP271 | HP277 | HP294 | HP295 | HP299 |
|-------------|------------|-------|-------|-------|-------|--------|-------|-------|
| OMZ | 0.625 | 2.5 | 2.5 | 2.5 | 0.625 | 0.625 | 0.625 | 1.25 |
| Co(II)–OMZ | 0.019 | 0.16 | 1.25 | 0.019 | 0.019 | 0.3125 | 1.25 | 0.019 |
| Fe(III)–OMZ | 1.250 | 2.5 | 2.5 | 0.625 | 0.625 | 1.25 | 2.5 | 2.5 |
| CLA | S | R | S | S | R | R | R | S |
| MTZ | S | R | S | R | R | R | R | S |

S: susceptible, R: resistant.

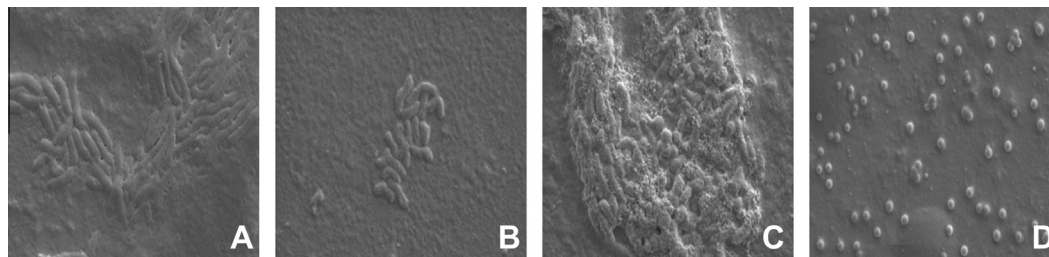


Fig. 9. SEM images of (A) HP270 control strain, HP270 strain treated with (B) OMZ, (C) Fe(III)–OMZ and (D) Co(II)–OMZ.

3.7. Solubility and microbiological assays

3.7.1. Solubility determination

The solubility values (see Fig. S4) of the complexes showed that the metal complexes are less soluble than OMZ. The solubility of the pure ligand in 0.1 N HCl pH 1 was 1.02 ± 0.08 mg mL⁻¹ while the solubilities of Fe(III)–OMZ and Co(II)–OMZ, were 0.32 ± 0.02 mg mL⁻¹ and 0.55 ± 0.04 mg mL⁻¹, respectively.

3.7.2. MIC values determination

OMZ and its metal complexes showed antimicrobial activity in all strains tested with a MIC₅₀ for reference strain (NCTC 11638) of 0.625 mg mL⁻¹ for OMZ, 0.019 mg mL⁻¹ for Co(II)–OMZ and 1.25 mg mL⁻¹ for Fe(III)–OMZ (Table 5). The MIC of Co(II)–OMZ of the reference strain was about 32 times lower than that of OMZ, while that for Fe(III)–OMZ was about two times higher. The antimicrobial activity obtained for OMZ against *H. pylori* strain is similar to that obtained by Mirshahi et al. [50]. The reference strain was susceptible to both CLA and MTZ; while the clinical isolated strains resulted resistant in the concentration ranges of 4–32 μg mL⁻¹ for CLA and 8–64 μg mL⁻¹ for MTZ.

The increased activity of Co(II)–OMZ is in line with previous studies of Co(II), Fe(III) and other metal ions as growth inhibitor agents of *H. pylori* [51]. These authors found that the activity of Co(II) cation against *H. pylori* is likely through a competition with Ni(II) either for the active metal binding site of the urease enzyme or for the nickel transport system that is unique to *H. pylori*. In contrast, Fe(III) ions showed no bacterial growth inhibition, in agreement with the higher MIC found by us for Fe(III)–OMZ. Although the inhibitory activity of Fe(III)–OMZ is lower than that of OMZ, it is better than that showed by the Fe(III) chloride reported [51]. The difference in the observed MIC values can only be associated to the nature of the metal ion of each complex and the distinctive action of Co(II) could be the basis of a new selective therapy for the treatment of *H. pylori* infection.

SEM observation revealed the efficacy of the Co(II)–OMZ complex action in inhibiting the *H. pylori* growth. Fig. 9A shows the uniform rod-shaped normal *H. pylori* cells, whereas the cells treated with OMZ and the Fe(III) and Co(II) complexes showed expected morphological changes in their cell membrane. Free OMZ and Fe(III)–OMZ (Fig. 9B and C, respectively) showed similar smaller shapes bacillary, but in OMZ the size of bacteria is lower than

Fe(III)–OMZ in according to the MIC values reported in Table 5. Moreover, coccoid forms were observed in Co(II)–OMZ complex indicating the morphological changes of *H. pylori*. These results were also substantiated by viability test using Live Dead viability Kit, which indicated the loss of 85% viability upon treatment with Co(II)–OMZ complex supporting the antimicrobial nature by damaged membranes (data not show).

4. Conclusions

Metal complexes of OMZ with Fe(III) and Co(II) with formulas [Fe(H₂O)₂(OMZ)₂]Cl₃·H₂O and [Co(H₂O)₂(OMZ)₂]Cl₂·H₂O were synthesized and characterized. UV–Visible, magnetic measurements, Mössbauer, and EPR data indicate that the metal ions are six coordinated in a distorted octahedral geometry. FTIR analysis showed that the complexation process is carried out by N_{BZ} and the O atom of the sulfoxide group. These experimental data are in line with DFT calculations, as N_{BZ} has a higher negative charge density, when coplanar with the sulfoxide group, than N_{PYR}. Moreover, the electrostatic potential map shows a higher surface of negative charge density over conformer B than conformer P. This fact confirms that coordination is performed by N_{BZ}, forming a five-membered chelate ring. Although the solubility of the Co(II)–OMZ complex was lower than that of the pure ligand, microbiological assays show that the MIC of Co(II)–OMZ is about 32 times lower than that of OMZ indicating a potential and promising application in the treatment of gastric pathologies associated with *H. pylori*. The SEM analysis in addition to the viability test on the *H. pylori* treated with the metal-complexes support the antimicrobial nature of Co(II)–OMZ by injury in the cell membrane.

Acknowledgments

The authors thank to Consejo Nacional de Investigaciones Científicas y Técnicas (CONICET: PIP 112-201101-00912), Universidad Nacional de San Luis (SECYT-UNSL Project 2-1612), Universidad Nacional de La Plata (UNLP), Universidad Nacional del Litoral, and MINCyT (PICT 2011-1654), Republica Argentina, for financial support. C.D.B., R.M. and G.E.N. are members of the CONICET. M.G.R. and E.G.V.H. thank CONICET for a fellowship.

Appendix A. Supplementary material

Supplementary data associated with this article can be found, in the online version, at <http://dx.doi.org/10.1016/j.molstruc.2013.12.073>.

References

- [1] Y. Zhang, K. Cai, X. Lang, X. Qiao, X. Li, *Environ. Pollut.* 166 (2012) 48–56.
- [2] C. Benedetta, A. Cesaretti, F. Elisei, *Phys. Chem. Chem. Phys.* 14 (2012) 823–834.
- [3] M.S. Refat, *J. Mol. Struct.* 1037 (2013) 170–185.
- [4] S. Sumathi, P. Tharmaraj, C.D. Sheela, C. Anitha, *Spectrochim. Acta A* 97 (2013) 377–383.
- [5] M. Baranska, E. Gumienna-Kontecka, H. Kozłowski, L.M. Proniewicz, *J. Inorg. Biochem.* 92 (2002) 112–120.
- [6] M. Baranska, W. Lasocha, H. Kozłowski, L.M. Proniewicz, *J. Inorg. Biochem.* 98 (2004) 995–1001.
- [7] D.U. Miodragović, G.A. Bogdanović, Z.M. Miodragović, M.D. Radulović, S.B. Novaković, G.N. Kaluderović, H. Kozłowski, *J. Inorg. Biochem.* 100 (2006) 1568–1574.
- [8] Y.Y. Bao, Q.X. Zhou, Y. Wan, Q.A. Yu, X.J. Xie, *Soil. Sci. Soc. Am. J.* 74 (2010) 1553–1561.
- [9] Y.P. Zhao, J.J. Geng, X.R. Wang, X.Y. Gu, S.X. Gao, *J. Colloid Interface Sci.* 361 (2011) 247–251.
- [10] B. Wen, R.X. Huang, P. Wang, Y.P. Zhou, X.Q. Shan, S.Z. Zhang, *Environ. Sci. Technol.* 45 (2011) 4339–4345.
- [11] E.K. Efthimiadou, Y. Sanakis, C.P. Raptopoulou, A. Karaliota, N. Katsaros, G. Psomas, *Bioorg. Med. Chem. Lett.* 16 (2006) 3864–3867.
- [12] W.A. Zordok, W.H. El-Shwiniy, M.S. El-Attar, S.A. Sadeek, *J. Mol. Struct.* 1047 (2013) 267–276; M.P. Lopez-Gresa, R. Ortiz, L. Perelló, J. Latorre, M. Liu-González, S. García-Granada, M. Pérez-Priede, M. Cantón, *J. Inorg. Biochem.* 92 (2002) 65–74.
- [13] G.G. Mohamed, F.A. Nour El-Dien, S.M. Khalil, A.S. Mohammad, *J. Coord. Chem.* 62 (2009) 645–654.
- [14] M.S. Refat, I.M. El-Deen, Z.M. Anwer, S. El-Ghol, *J. Coord. Chem.* 62 (2009) 1709–1718.
- [15] D.Y. Lee, H.S. Shin, S.K. Bae, M.G. Lee, *Biopharm. Drug Dispos.* 27 (2006) 209–218.
- [16] P.J. Unge, *J. Gastroenterol.* 33 (1998) 48–52.
- [17] A. Zullo, V. De Francesco, C. Hassan, L. Ridola, A. Repici, V. Bruzzese, D. Vaira, *Digest Liver Dis* 45 (2013) 18–22.
- [18] H. Seddik, S. Ahid, T. El Adioui, F.-Z. El Hamdi, M. Hassar, R. Abouqal, Y. Cherrah, A. Benkirane, *Eur. J. Clin. Pharma.* (2013) 1–7, <http://dx.doi.org/10.1007/s00228-013-1524-6>.
- [19] D.G. Rancourt, A.M.Mc. Donald, A.E. Lalonde, J.Y. Pyng, *Am. Miner.* 78 (1993) 1–7.
- [20] K. Lagarec, D.G. Rancourt, *Mössbauer Spectral Analysis Software, Version 1.0*, Department of Physics, University of Ottawa, 1998.
- [21] M.J. Frisch, G.W. Trucks, H.B. Schlegel, G.E. Scuseria, M.A. Robb, J.R. Cheeseman, J.A. Montgomery, T. Vreven, K.N. Kudin, J.C. Burant, J.M. Millam, S.S. Iyengar, J. Tomasi, V. Barone, B. Mennucci, M. Cossi, G. Scalmani, N. Rega, G.A. Petersson, H. Nakatsuji, M. Hada, M. Ehara, K. Toyota, R. Fukuda, J. Hasegawa, M. Ishida, T. Nakajima, Y. Honda, O. Kitao, H. Nakai, M. Klene, X. Li, J.E. Knox, H.P. Hratchian, J.B. Cross, C. Adamo, J. Jaramillo, R. Gomperts, R.E. Stratmann, O. Yazyev, A.J. Austin, R. Cammi, C. Pomelli, J.W. Ochterski, P.Y. Ayala, K. Morokuma, G.A. Voth, P. Salvador, J.J. Dannenberg, V.G. Zakrzewski, S. Dapprich, A.D. Daniels, M.C. Strain, O. Farkas, D.K. Malick, A.D. Rabuck, K. Raghavachari, J.B. Foresman, J.V. Ortiz, Q. Cui, A.G. Baboul, S. Clifford, J. Cioslowski, B.B. Stefanov, G. Liu, A. Liashenko, P. Piskorz, I. Komaromi, R.L. Martin, D.J. Fox, T. Keith, M.A. Al-Laham, C.Y. Peng, A. Nanayakkara, M. Challacombe, P.M.W. Gill, B. Johnson, W. Chen, M.W. Wong, C. Gonzalez, J.A. Pople, *Gaussian 03 Revision B.05*, Gaussian Inc, Wallingford, CT, 2003.
- [22] A.D. Becke, *J. Chem. Phys.* 98 (1993) 5648–5652.
- [23] C. Lee, W. Yang, R.G. Parr, *Phys. Rev. B* 37 (1988) 785–789.
- [24] P.M. Bhatt, G.R. Desiraju, *Chem. Commun.* (2007) 2057–2059, CCDC 633382.
- [25] W.J. Hehre, R. Ditchfield, J.A. Pople, *J. Chem. Phys.* 56 (1972) 2257–2261.
- [26] E.D. Glendening, A.E. Reed, J.E. Carpenter, F. Weinhold, *NBO Version 3.1*, 1993.
- [27] M. Gómez-Gallego, I. Fernández, D. Pellico, A. Gutierrez, M.A. Sierra, J.J. Lucena, *Inorg. Chem.* 45 (2006) 5321–5327.
- [28] M. Cossi, G. Scalmani, N. Rega, V. Barone, *J. Chem. Phys.* 117 (2002) 43–54.
- [29] J. Tomasi, B. Mennucci, R. Cammi, *Chem. Rev.* 105 (2005) 2999–3094.
- [30] Y. Kawakami, K. Oana, M. Hayama, H. Ota, M. Takeuchi, K. Miyashita, T. Matsuzawa, K. Kanaya, *Int. J. Med. Sci.* 3 (2006) 112–116.
- [31] C.W. Howden, *Clin. Pharmacokinetics* 20 (1990) 39–49.
- [32] S.H. Tarulli, O.V. Quinzani, O.E. Piro, E.E. Castellano, E.J. Baran, *J. Mol. Struct.* 797 (2006) 56–60.
- [33] M. Tahir Güllüoğlu, Ö. Mustafa, K. Mustafa, S. Kalaiichelvan, N. Sundara ganesan, *Spectrochim. Acta A* 76 (2010) 107–114.
- [34] K.J. Morgan, *J. Chem. Soc. A* (1961) 2343–2347.
- [35] N. Sultana, A. Naz, M. Saeed Arayne, M. Ahmed Mesaik, *J. Mol. Struct.* 969 (2010) 17–24.
- [36] R.R. Amin, Y.B. Yamany, *J. Mol. Struct.* 1008 (2012) 54–62.
- [37] S.M.E. Khalil, H.F.O. El-Shafiy, *Synth. React. Inorg. Met. Org. Chem.* 30 (2000) 1817.
- [38] A.B.P. Lever, *Inorganic Electronic Spectroscopy*, second ed., Elsevier Science Publishing Company, Amsterdam, 1984.
- [39] M. Shebl, S.M.E. Khalil, F.S. Al-Gohani, *J. Mol. Struct.* 980 (2010) 78–87.
- [40] A.A.A. Emara, *Spectrochim. Acta A* 77 (2010) 117–125.
- [41] K.R. Choi, T. Kouth, S.J. Kim, C.S. Kim, *Phys. Status Solidi B* 244 (2007) 4582–4585.
- [42] J. Zarembowitch, O. Kahn, *Acid Inorg. Chem.* 23 (1984) 589–593.
- [43] A.C. Rizzi, C.D. Brondino, R. Calvo, R. Baggio, M.T. Garland, R.E. Rapp, *Inorg. Chem.* 42 (2003) 4409–4416.
- [44] K.P. Guerra, R. Delgado, *Polyhedron* 27 (2008) 2265–2270.
- [45] International Centre for Diffraction Data, *JPCDS, database. PDF-2*, 2003.
- [46] A.N.M.A. Alagha, A.G. Al-Sehemi, T.M. El-Gogary, *Spectrochim. Acta A* 95 (2012) 414–422.
- [47] D. Sanna, C.G. Ágoston, G. Micera, I. Sóvágó, *Polyhedron* 20 (2001) 3079–3090.
- [48] N. Yasarawan, K. Thipyapong, S. Sirichai, V. Ruangpornvisuti, *J. Mol. Struct.* 1031 (2013) 144–151.
- [49] G. Orpen, L. Brammer, F.H. Allen, O. Kennard, D.G. Watson, R. Taylor, *Chem. Soc. Dalton Trans.* (1987) S1–S83.
- [50] F. Mirshahi, G. Fowler, A. Patel, G. Shaw, *J. Clin. Pathol.* 51 (1998) 220–224.
- [51] S.F.A. Bruggaber, G. French, R.P.H. Thompson, J.J. Powell, *Helicobacter* 9 (2004) 422–428.